Journal of Fluorescence (2019) 29:1079–1087
https://doi.org/10.1007/s10895-019-02419-8

ORIGINAL ARTICLE

Fast and Reversible "Turn on" Fluorescent Sensors Based on Bisphenol-a for Zn^{2+} in Aqueous Solution

Begum Tabakci[1] · Hayder Mahdi Ahmed Ahmed[1] · Serkan Erdemir[1]

Received: 1 March 2019 / Accepted: 8 July 2019 / Published online: 24 July 2019

Abstract

Two novel bisphenol-A derivatives (**R1** and **R2**) linked pyrene and napthylthiazole moieties were synthesized via condensation reaction, and positively applied for the selective recognition of Zn^{2+} ion in EtOH/H_2O. Their optical properties were observed by using UV-vis and fluorescence measurements. **R1** and **R2** exhibited high selectivity and sensitivity towards Zn^{2+} over other metal ions. This fluorescence selectivity may be owing to inhibited excited-state intramolecular proton transfer (ESIPT) and photoinduced electron transfer (PET). The fluorescence titration analysis indicated detection limits of **R1** and **R2** for Zn^{2+} at 17.5 nM and 0.94 μM, respectively. Moreover, **R1** and **R2** were successfully applied to the detection of Zn^{2+} with different concentrations in water samples.

Keywords Fluorescence · Turn on · Bisphenol a · Zinc

Introduction

Zinc is a known trace element and cofactor of more than 300 human metalloenzymes involved in many physiological processes [1]. Moreover, its potential therapeutic activity for the treatment of various diseases is extensively investigated. However, many physiological and therapeutic mechanisms of action of zinc are not yet well understood, as the d10 configuration of Zn^{2+} hinders detection by usual spectroscopic techniques [2–5]. Modern industrial development has caused elevated concentrations of heavy metals, including Zn^{2+}, which leads to toxicity of soil and inhibits plant and animal growth. Although Zn^{2+} plays vital roles in physiological and pathological processes [6], excessive amounts of zinc in human cause many severe diseases such as Alzheimer's disease [7], ischemic stroke [8] and epilepsy [9]. Thus, there is a need for rapid response, effective detection and reliable identification of trace levels of Zn^{2+} in the environment and biological samples. In this sense, the development of fluorescent sensors for the detection of zinc constitutes a very active field of research. In addition, fluorescence as a signaling technique outstrips other techniques in terms of simplicity, sensitivity and selectivity [10–16].

Fluorescent sensors are commonly composed of two structural subunits: a fluorophore and an ionophore, and both are connected through a spacer or also known as a linker [17, 18]. So far, fluorescence sensors bearing different fluorophores for Zn^{2+} have been reported, such as rhodamine [19], coumarin [20], BODIPY [21], fluorescein [22]. Bisphenol A (BPA), chemically designated as 2,2-bis(4-hydroxyphenyl) propane is an endocrine disrupting chemical, and although it is commonly used as intermediate in variety of consumer products like polycarbonate plastics and epoxy resins [23], the use of bisphenol-A as fluorophore is very scarce [24, 25]. Therefore, we think that the Schiff base (C=N) derivatives of bisphenol-A as fluorophore and pyrene or naphthylthiazole units as ionophores would be interesting to detect metal ion. In the excited states, an unfixed C=N structure is non-fluorescent owing to the predominant decay process of C=N isomerization [26]. After complexation with metal ions, its fluorescence increases strongly since it restricts the rotation of the C=N bond, which induce to the suppression of C=N isomerization.

We herein reported the synthesis and Zn^{2+} recognition properties of two new bisphenol-A based on fluorescent receptors (R1 and R2). Receptors **R1** and **R2** exhibited selective

Electronic supplementary material The online version of this article (https://doi.org/10.1007/s10895-019-02419-8) contains supplementary material, which is available to authorized users.

✉ Serkan Erdemir
serdemir82@gmail.com

[1] Science Faculty, Department of Chemistry, Selcuk University, 42031 Konya, Turkey

emission responses to Zn^{2+} in a mixture of EtOH/H_2O solution with low detection limits.

Experimental

Materials and Method

The chemicals used in experiments were purchased from commercial suppliers. ^{1}H NMR (Proton Nuclear Magnetic Resonance), ^{13}C NMR (Carbon Nuclear Magnetic Resonance), COSY (Correlation Spectroscopy) and APT (Attached Proton Test) spectra were recorded on Varian 400 MR in DMSO-d_6 (Dimethyl sulfoxide-d_6) and $CDCl_3$ (Chloroform-d) as solvents. Bruker FTIR (Fourier-Transform Infrared Spectroscopy) instrument was used to FTIR spectra analysis. Absorption spectra were measured by using a Shimadzu 1280 ultraviolet visible spectrophotometer at room temperature. A Perkin Elmer LS 55 instrument was used for fluorescence studies. The fluorescence spectra were recorded with the excitation wavelength of 365 nm by 5 nm slit. All pH measurements were made with a Crison Basic 20 pH meter.

Synthesis Procedure of R1 and R2

The bisphenol A-dialdehyde (1) was synthesized according to the method reported in the previous work [25]. Then, to a solution of bisphenol-A dialdehyde (0.2 g, 0.70 mmol) in 30 mL ethanol, 1-pyrenemethylamine hydrochloride (0.38 g, 1.44 mmol) in the presence of triethylamine or 4-(naphthalen-2-yl)thiazol-2-amine (0.32 g, 1.44 mmol) were added, and the mixture was stirred for 4 h at room temperature. At the end of this period, yellow residue was obtained and washed with anhydrous ethanol for three times, dried to give receptor **R1** and **R2** as yellow solids.

R1: Yield: % 81; Mp: 163–164 °C; FTIR (ATR): 1633 (C=N) cm^{-1}; ^{1}H NMR (400 MHz $CDCl_3$): δ 13.35 (s, 2H), 8,31 (s, 2H), 8.26 (d, 2H, J = 9.39 Hz), 8.17 (d, 4H, J = 7.82 Hz), 8.10–8.14 (m, 4H), 8.03 (d, 4H, J = 2.15 Hz), 7.97–8.01 (m, 2H), 7.90 (d, 2H, J = 8.02 Hz), 7.09, 7.10 (dd, 2H, J = 2.54, 2.34 Hz), 6.97 (d, 2H, J = 2.34 Hz), 6.81 (d, 2H, J = 8.80 Hz), 5.45 (s, 4H), 1.54 (s, 6H).^{13}C NMR (100 MHz $CDCl_3$): δ 165.86, 158.97, 140.87, 131.29, 131.21, 131.12, 131.06,130.79, 129.28, 128.88, 128.16, 127.41, 126.88, 126.08, 125.39, 125.33, 124.99, 124.90, 124.76, 122.94, 118.18, 116.66, 60.55, 41.50, 30.91. Anal. Calcd for $C_{51}H_{38}N_2O_2$: % C, 86.17; H, 5.39; N, 3.94. Found: % C, 86.28; H, 5.41; N, 4.01.

R2: Yield: % 76; Mp: 158–160 °C; FTIR (ATR): 1652 (C=N), 1624 (C=N) cm^{-1}; ^{1}H NMR (400 MHz d_6-DMSO): δ 11.46 (s, 2H), 9,39 (s, 2H), 8.53 (s, 2H), 8.16 (s,2H), 8.09 (d, 2H, J = 8.8 Hz), 7.88–7.99 (m, 8H), 7.47–7.52 (m, 4H), 7.31 (d, 2H, J = 8.8 Hz), 6.94 (d, 2H, J = 8.8 Hz), 1.68 (s, 6H). ^{13}C NMR (100 MHz d_6-DMSO): δ 171.27, 164.50, 158.92, 152.93, 141.90, 134.48, 133.65, 133.19, 131.85, 128.76, 128.08, 127.05, 126.80, 125.25, 124.47, 119.28, 117.28, 114.26, 41.86, 30.89. Anal. Calcd for $C_{43}H_{32}N_4O_2S_2$: % C, 73.69; H, 4.60; N, 7.99; S, 9.15. Found: % C, 73.88; H, 4.67; N, 8.01; S, 9.18

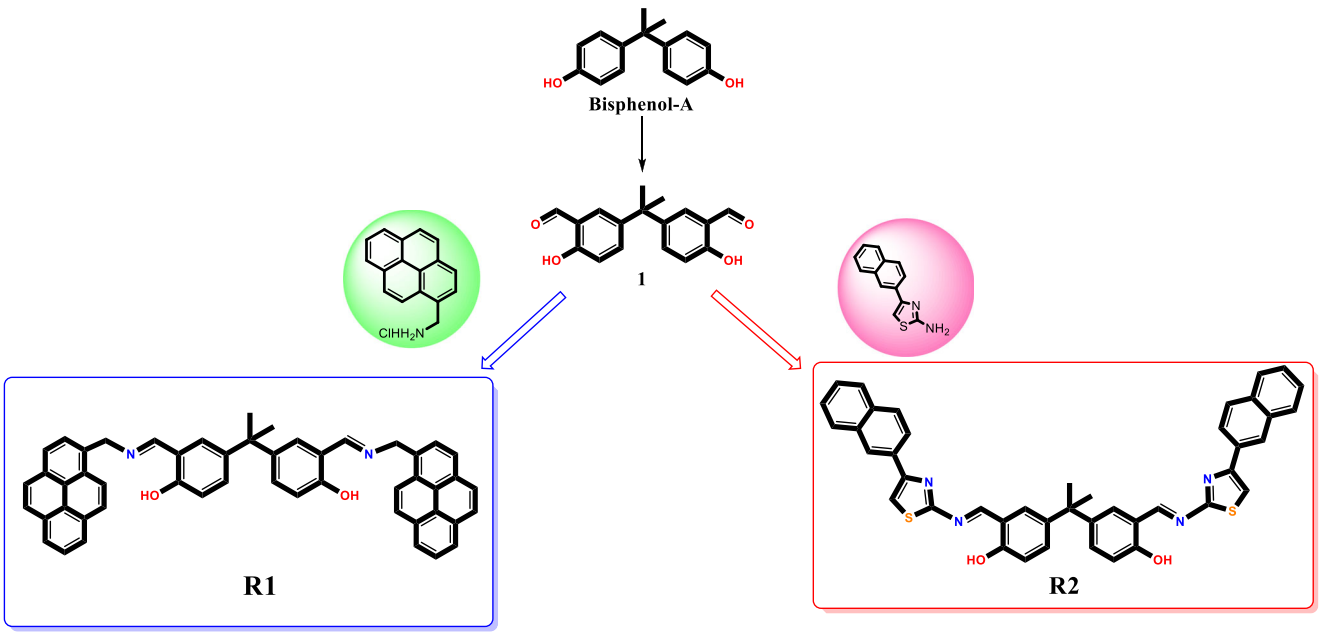

Scheme 1 Synthesis route for receptors **R1** and **R2**

Analytical Procedure

The stock solutions of **R1** and **R2** were prepared at concentration of 0.2 μM and 5.0 μM for fluorescence and 10 μM and 20 μM for UV-vis measurements in EtOH/H_2O (95/5, *v*/v), respectively. Solutions of metal ions as perchlorate salts were prepared in H_2O with a concentration of 0.001 M for UV–vis absorption and fluorescence spectra analysis. Titration experiments were realized in 3 mL solution of **R1** and **R2** by addition of increasing metal ion concentration. The fluorescence spectra were performed with the excitation wavelength at 365 nm, slit 5.0/5.0 nm. To monitor the chemical shifts arising from the interaction of **R1** and **R2** with Zn^{2+}, ^{1}H NMR experiments were also realized by addition of the known quantity of Zn^{2+} ion to solutions of **R1** (0.07 M) and **R2** (0.07 M).

Results and Discussion

As shown in Scheme 1, **R1** and **R2** were synthesized via the condensation reaction of the aldehyde derivative of bisphenol-A (1) and pyrenemethylamine hydrochloride or 4-(naphthalen-2-yl)thiazol-2-amine in ethanol at room temperature, respectively. The formation of R1 and R2 was confirmed by appearance of imine protons at δ 8.31 and δ 9.39 ppm in ^{1}H NMR spectra (Fig. 1). The structures were also supported by ^{1}H NMR and ^{13}C NMR, COSY, APT, FTIR and elemental analysis (Fig. S1–S10).

Metal Ion Selectivity and Competitiveness of R1 and R2

The fluorescence properties of receptors **R1** and **R2** were observed in the presence of different metal ions in a mixture

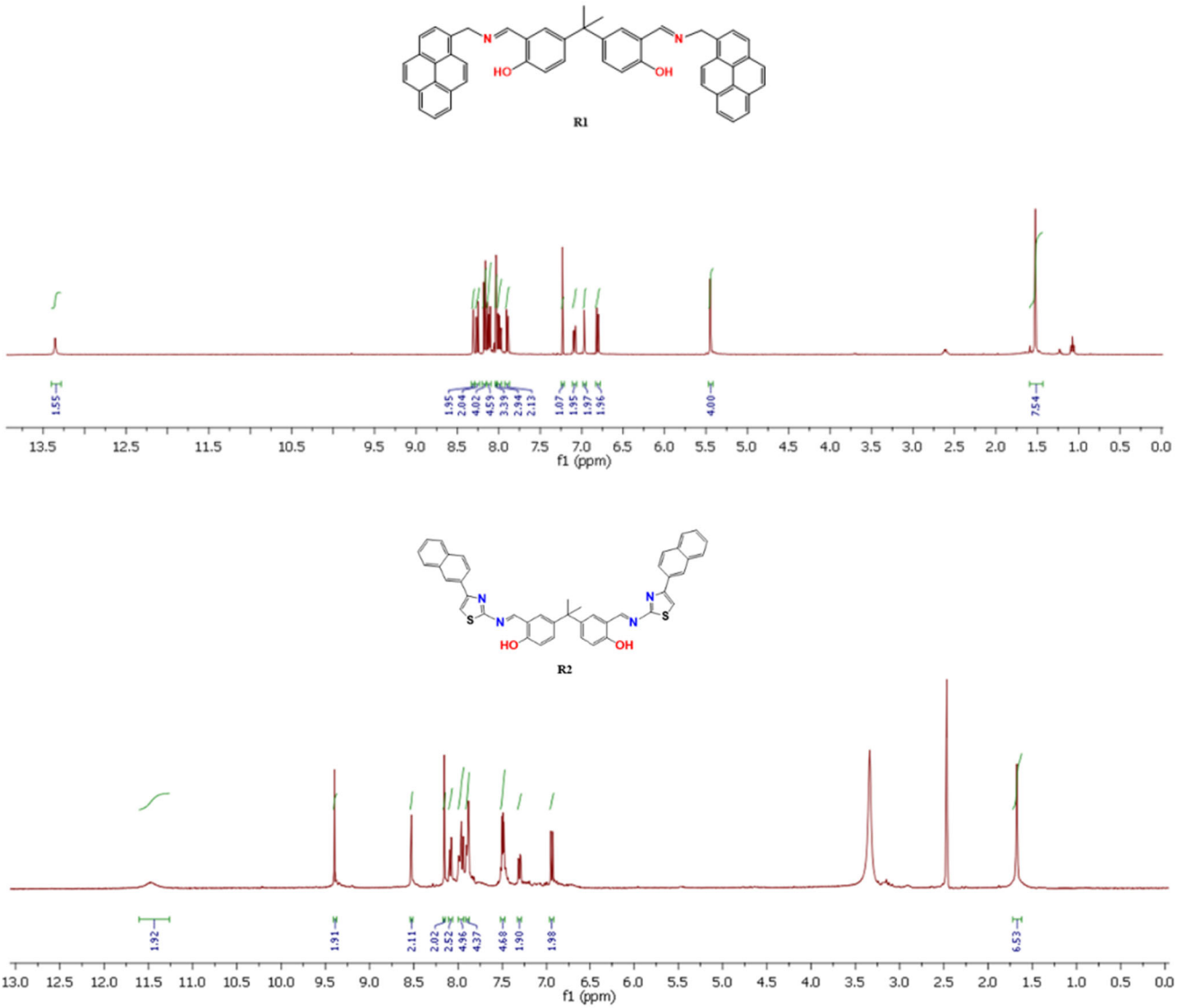

Fig. 1 ^{1}H NMR spectra of R1 and R2 in $CDCl_3$

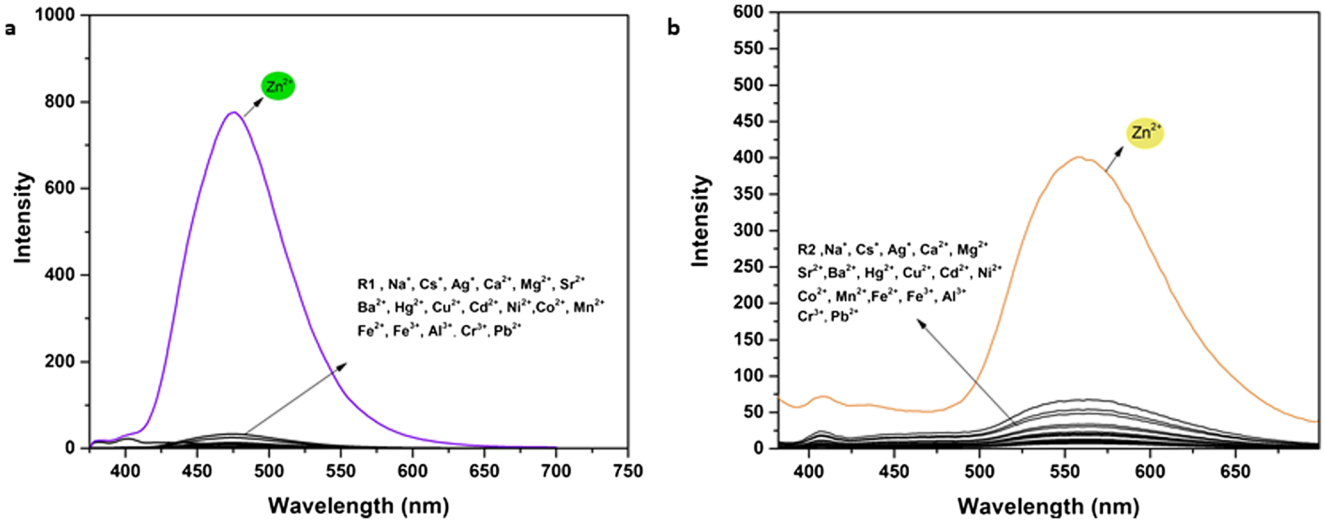

Fig. 2 Fluorescence spectra of (**a**) **R1** (0.2 μM) and (**b**) **R2** (5.0 μM) in EtOH/H_2O (95/5, *v*/v), in the presence of various metal ions

of EtOH/H_2O (95/5, *v*/v) solution. Receptors **R1** and **R2** exhibited any emission band at range of 400–700 nm. This phenomenon might be interested with the combined PET (Photo-induced electron transfer) effect and ESIPT (Excited state intramolecular proton transfer) process in the excited state. However, the addition of Zn^{2+} (5.0 equiv.) caused a dramatic fluorescence enhancement at 472 nm for **R1** and 560 nm for **R2** (Fig.2a, b), showing formation of R1-Zn^{2+} and R2-Zn^{2+} complexes. After the complexation, the PET process and ESIPT might be inhibited, leading to fluorescence

Fig. 3 Visual fluorescence changes upon addition of various metal ions to **R1** and **R2** solutions

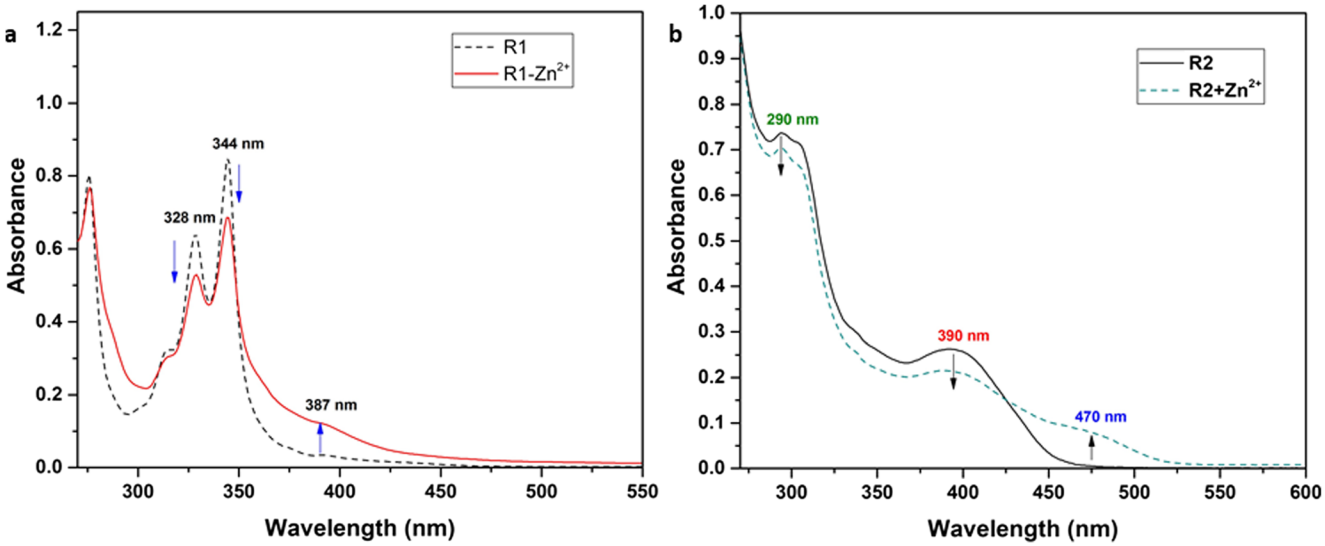

Fig. 4 UV–vis changes of (**a**) **R1** (10 μM) and (**b**) **R2** (20 μM) with 2.0 equiv. of Zn^{2+} in EtOH/H_2O (95/5, v/v)

enhancement. When other common metal ions were added to the solution of **R1** and **R2**, no obvious fluorescent changes were observed under the same conditions. In addition, initiatory test for the detection of Zn^{2+} was performed as fluorometric test in UV light. As seen in Fig. 3, **R1** and **R2** was suddenly emitted blue and yellow fluorescent with Zn^{2+} among other metal ions, respectively. Otherwise, in the UV–vis studies (Fig. 4), whereas **R1** indicated three main absorbance bands at 275, 328 and 344 nm, and **R2** indicated two bands at 290 and 390 nm. When Zn^{2+} ion was added to solutions of **R1** and **R2**, these bands decreased and new absorbance bands were revealed at 387 nm for **R1** and 470 nm for **R2**, indicating formation of R1–Zn^{2+} and R2–Zn^{2+} complexations (Fig.4a, b).

The fluorescence titration spectra of **R1** and **R2** in presence of different added concentrations of Zn^{2+} were depicted in Fig. 5. As the concentration of Zn^{2+} was increased (0–5 equiv.), there was distinct emission enhancing of the bands centred at 472 nm for **R1** and 560 nm for **R2**, which showed the isomerization of C=N bond, increased the rigidity of the molecule, and produced the chelated enhanced fluorescence (CHEF) effects [27]. With the concentration of Zn^{2+} ions up to 2.0 equiv., the fluorescence intensities of **R1** and **R2** were gradually increased, and then the fluorescence intensity did not increase any further and a plateau was reached. To reveal the stoichiometry ratios of **R1** and **R2** with Zn^{2+}, Job's plot experiments were realized. In Fig. 6, the emission intensities at 472 and 560 nm are plotted against the molar fractions of **R1** and **R2**, respectively. The emission intensities at 472 and 560 nm were reached maximum at 0.33 of molar fractions of **R1** and **R2**, showing 1:2 stoichiometries of **R1** and **R2** with Zn^{2+} (Fig. 6). The values of the linearly dependent coefficient

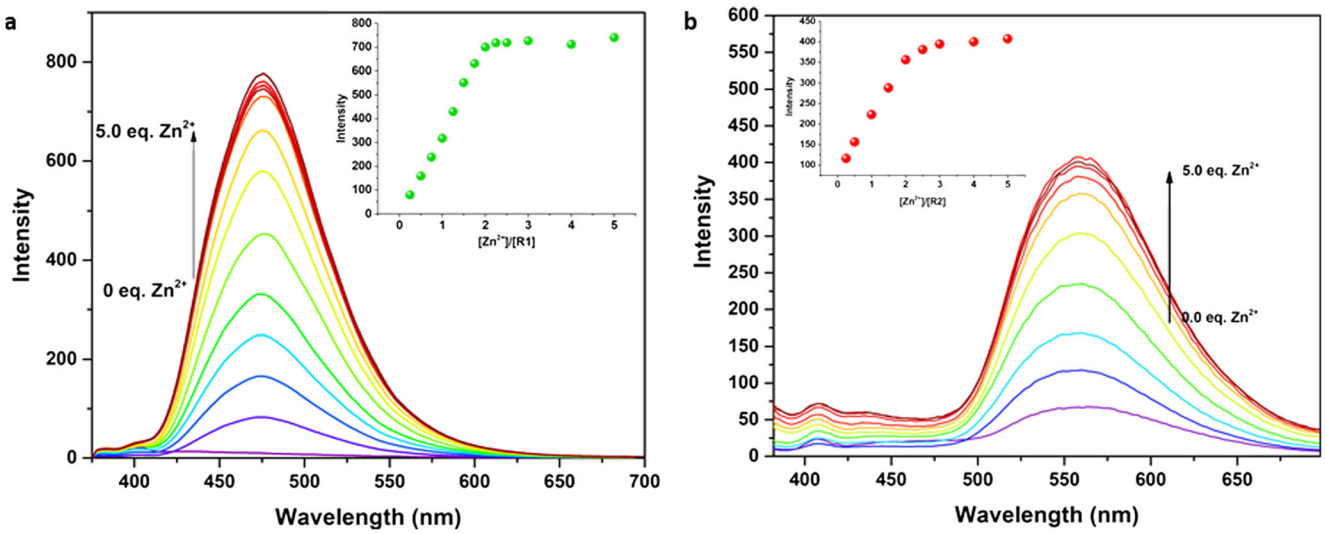

Fig. 5 Fluorescence changes of (**a**) **R1** and (b) **R2** with various amounts of Zn^{2+} (0.0–5.0 equiv.) in EtOH/H_2O (95/5, v/v) (insets in a and (**b**) titration profile indicate the formation of a 1:2 complex

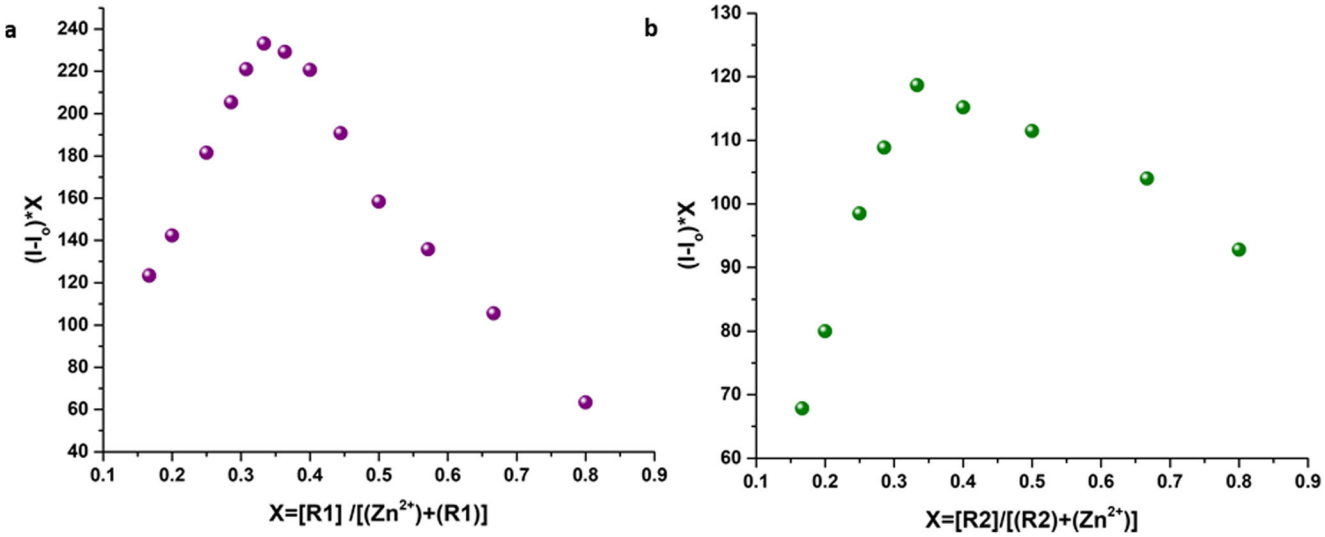

Fig. 6 Job plots of R1-Zn^{2+} (**a**) and R2-Zn^{2+} (**b**) complexations

(R^2) were found to be 0.99, and the detection limits by fluorescent titration data were also calculated as 17.5 nM for **R1** and 0.94 μM for **R2** with 3σ/slope, (Fig. S11). Based on 1:2 binding stoichiometry, the binding constants (logK) for **R1** and **R2** towards Zn^{2+} ion was calculated using the Benesi-Hildebrand eq. [28] and found to be 13.46 and 10.68, respectively (Fig. S12).

Considering multiple metal ions in samples, fluorescence interference experiments for **R1** and **R2** were subsequently carried out in presence of various competing metal ions to explore the possibility of using **R1** and **R2** as a practical ion selective fluorescent sensor for Zn^{2+}. The effect of foreign metal ions on the fluorescence intensities of R1-Zn^{2+} and R2-Zn^{2+} systems was presented in Fig. S13. As seen in Fig. S13, the foreign metal ions did not interfere on the detection of Zn^{2+} by **R1** and **R2**. These results suggest that receptors **R1** and **R2** can be an excellent fluorescent sensor for sensing of Zn^{2+} ion with highly selectivity and anti-interference performance among the other relevant metal ions.

In addition, the energy-optimized structures of **R1** and **R2** were obtained on density functional theory (DFT) calculations at B3LYP/6-31G (d, p) level by using Gaussian 16 program [29–31]. The optimized structures, the energy of MOs and contours of selected HOMO and LUMO orbitals of **R1** and **R2** have been shown in Fig. 7. The HOMO was localized on pyrene ring in **R1**, while the LUMO was located on the pyrene and benzene in bisphenol-A. Meanwhile, the π electrons of HOMO of **R2** are mainly distributed on the bisphenol-A fragment. The LUMO is distributed on the napthylthiazole unit. The HOMO to LUMO energy gaps for **R1** and **R2** were determined as 3.327 eV and 1.631 eV, respectively. This difference in the energy gaps of **R1** and **R2** may ascribed to the lack of π-conjugation in **R1** unlike **R2**.

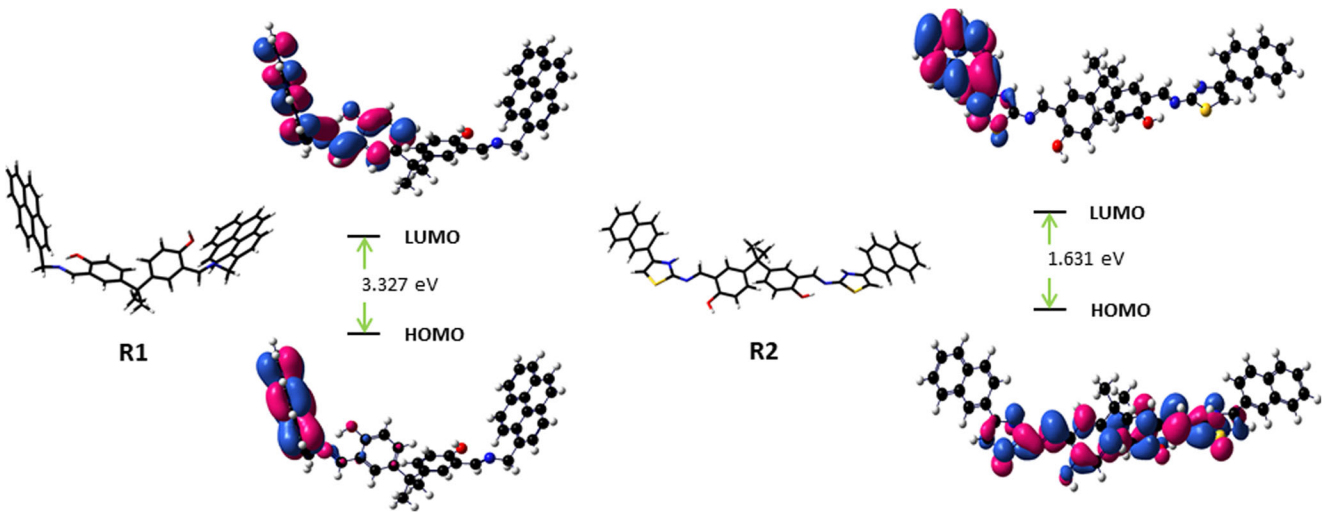

Fig. 7 Optimized structures and the HOMO and LUMO energy gaps levels of of **R1** and **R2**: Calculations are based on optimized ground state geometry by DFT at the B3LYP/6-31G (p,d) /level using Gaussian 16

Table 1 Determination of Zn^{2+} in the spiked tap water samples by the present method

Sample[a]	Added (μM)	Measured (μM)	Recovery (%)	RSD ($n = 3$) (%)
T1	5	4.97 (R1)	99.4	0.76
		4.79 (R2)	95.8	1.09
T2	10	10.07 (R1)	100.7	0.92
		9.89 (R2	98.9	1.03
T3	15	14.95 (R1)	99.6	1.22
		14.81 (R2	98.7	1.45

[a] T1-T3 are known concentrations of Zn^{2+} solution sample

Effect of pH and Reversibility Tests

Figure S14 shows the fluorescence intensities of **R1**, **R2** and their Zn^{2+} complexes at different pH in EtOH/H_2O (95/5, *v*/v). The pH of the solutions was adjusted using either NaOH or HCl solutions. The fluorescence intensities of **R1** and **R2** were not remarkably changed over the pH range tested. By the addition of Zn^{2+}, **R1** and **R2** solutions showed strong fluorescence emission in the range of pH 6 and 8. Nevertheless, the fluorescence intensities towards Zn^{2+} of **R1** and **R2** were apparently decreased at high pH 9.0, since -OH ions interacted with Zn^{2+} ions ($K_{sp} = 3 \times 10^{-17}$ for $Zn(OH)_2$) [32]. Consequently, these receptors would be an ideal sensor for monitoring Zn^{2+} in the pH range of 6–8.

To increase the applicability of sensors, the reversibility is a significant point in the design of novel optical sensors. Thus, we

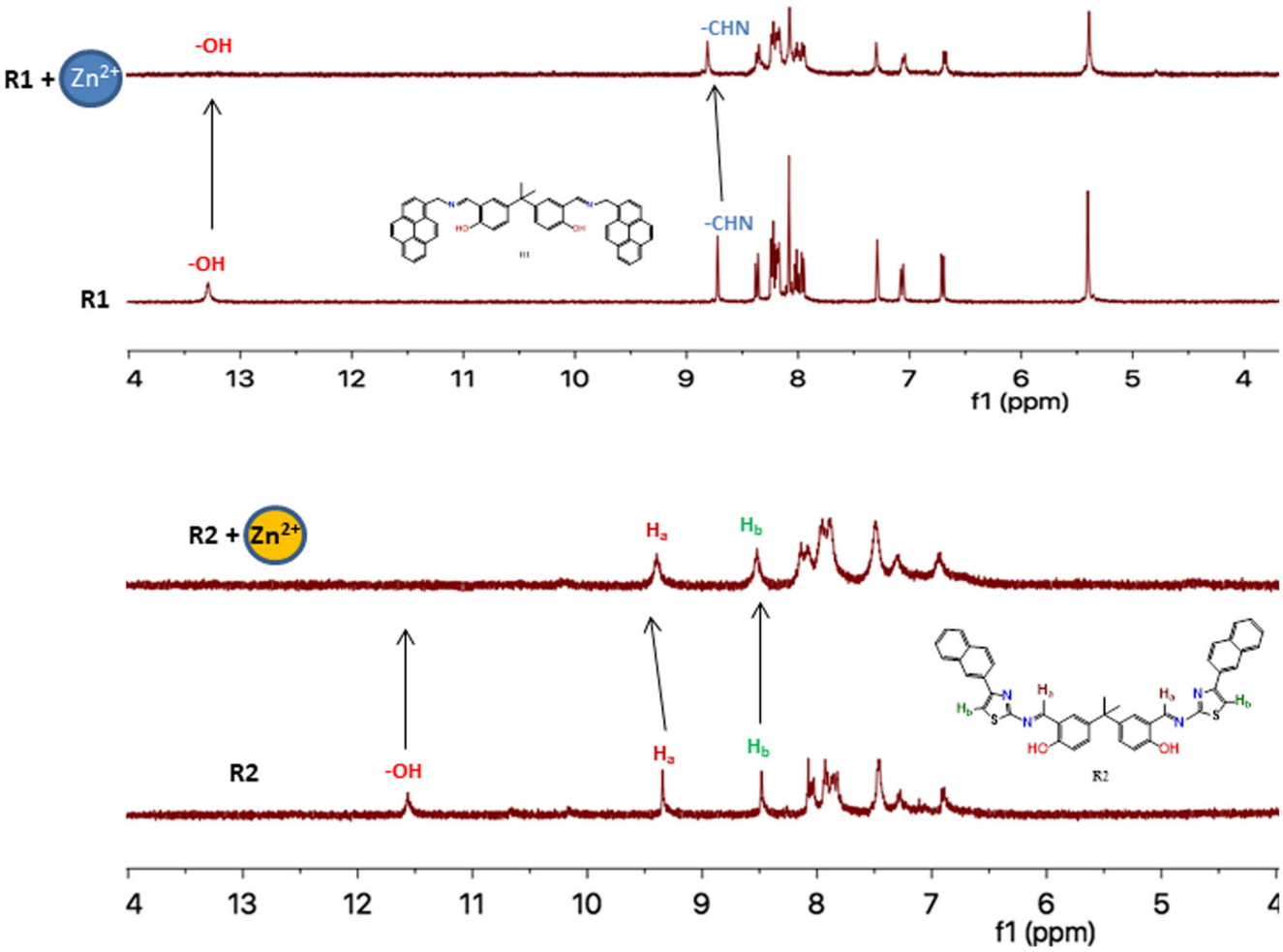

Fig. 8 ^1H NMR (400 MHz DMSO-d_6) spectra changes of **R1** and **R2** upon addition of Zn^{2+} (2.0 equiv.)

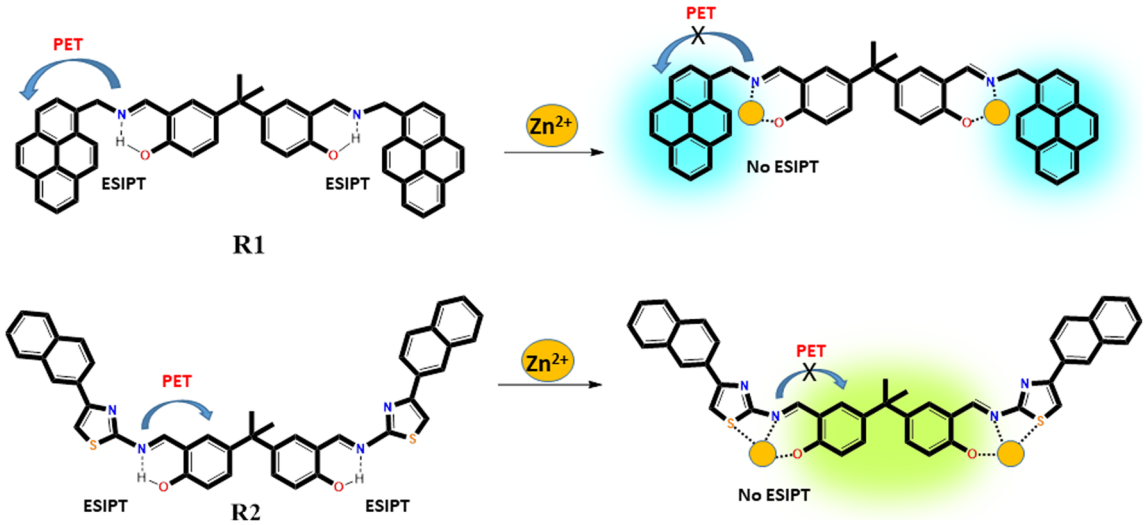

Scheme 2 The proposed interaction model between Zn^{2+} with R1 and R2

observed the reversibility of **R1** and **R2** for Zn^{2+} ion using EDTA solution. As seen in Fig. S15 and S16, an immediate fluorescence quenching was observed upon the addition of EDTA to R1-Zn^{2+} and R2-Zn^{2+} systems. Also, the fluorescence enhancing capability of **R1** and **R2** for Zn^{2+} kept relatively stable values within 4 cycles with little emission intensity loss (Fig. S15b and S16b). It could be found that EDTA could bleach the "signal-on" fluorescence emission bands for Zn^{2+}. Moreover, the response time of **R1** and **R2** for Zn^{2+} was performed, and the results were showed in Fig. S17. In the presence of Zn^{2+}, the fluorescence emission intensities of **R1** and **R2** reached the maximum values within 10 s, and remaining constant from 10 s to 5 min, which shows quickly responsive "turn-on" fluorescent sensor for Zn^{2+}. Moreover, to assess the practical efficacy of **R1** and **R2**, we used them to determine the concentration of Zn^{2+} in tap water samples. For this purpose, the water samples were centrifuged and filtrated, and then added to Zn^{2+} solutions with the concentrations of 5, 10 and 15 μM. Briefly, the Zn^{2+} spiked water sample (0.15 mL) was mixed with 2.85 mL of EtOH, then 0.6 μL for R1 and 15 μL for R2 of the EtOH solution of receptors (R1 or R2) was added and the fluorescence spectra was recorded. As shown in Table 1, the recovery was between 95.8% and 100.7% with lower relative standard deviation (RSD < 2%), which clearly shows the reliability and accuracy of the proposed method.

^{1}H NMR Experiments

To insight the binding interaction of receptors **R1** and **R2** with Zn^{2+}, ^{1}H NMR experiments were performed by addition of 2.0 equiv. Zn^{2+} ion to solutions of **R1** and **R2** in DMSO-d_6 (Fig. 8) In the ^{1}H NMR of the free **R1** and **R2**, the peaks at δ 13.28 or δ 11.56 ppm and δ 8.72 or δ 9.37 ppm correspond to the protons of phenolic-OH and imine groups, respectively. Upon the addition of Zn^{2+} with 2.0 equiv. concentration, the phenolic-OH signals at δ 13.28 and δ 11.56 ppm disappeared, indicating that OH was effective a group in the complexation between Zn^{2+} and **R1** or **R2**. Also, the signals of imine protons (CHN) at δ 8.72 ppm for **R1** and δ 9.37 ppm for **R2** shifted to 8.81 ppm and 9.40 ppm while Zn^{2+} existed. On the other hand, the CH signal (H_b) at δ 8.51 ppm belongs to thiazole moiety of **R2** was slightly downfield shifted to δ 8.54 ppm in presence of Zn^{2+}, suggesting thiazole ring-metal coordination. Very little change can be observed for the other aromatic protons. These data show that the phenolic-OH and imine for **R1**, and thiazole ring as well as the phenolic-OH and imine groups for **R2** are efficient on formation of their Zn^{2+}-complexes. According to these data, the proposed interaction models between Zn^{2+} with **R1** and **R2** were depicted in Scheme 2.

Conclusion

In summary, fluorescence sensing abilities of two novel synthesized receptors, i.e. **R1** and **R2** were explored for efficient, rapid and selective sensing of Zn^{2+}. Bisphenol-A based sensors (**R1** and **R2**), containing pyrene and napthylthiazole units, displayed high selectivity and sensitive towards Zn^{2+} ion with little interference observed from other coexistent metal ions. The 1:2 interactions between **R1** and **R2** of Zn^{2+} ion with detection limits 17.5 nM and 0.94 μM were proved from fluorescence spectral data, respectively. The achieved reversibility tests indicated that **R1** and **R2** could be reused with proper treatment. Moreover, the practical applicability of **R1** and **R2** in water samples for Zn^{2+} detection also makes them lucrative and worthwhile. These data exemplified a new possibility for the exploration of novel fluorescence sensors with high selectivity and specificity.

Acknowledgements We are grateful for the financial supports from the Research Foundation of Selcuk University (BAP) and The Scientific and Technical Research Council of Turkey (TUBITAK-Grant Number 117Y217) for financial support of this work.

References

1. Li K, Wang X, Tong A (2013) A 'turn-on' fluorescent chemosensor for zinc ion with facile synthesis and application in live cell imaging. Anal Chim Acta 776:69–73
2. Xie X, Smart TG (1991) A physiological role for endogenous zinc in rat hippocampal synaptic neurotransmission. Nature 349:521–524
3. Berg J, Shi Y (1996) Galvanization of biology: a growing appreciation for the roles of zinc. Science 271:1081–1085
4. Frederickson CJ, Koh JY, Bush AI (2005) The neurobiology of zinc in health and disease. Nat Rev Neurosci 6:449–462
5. Que EL, Domaille DW, Chang CJ (2008) Metals in neurobiology: probing their chemistry and biology with molecular imaging. Chem Rev 108:1517–1549
6. Liu Y, Zhang N, Chen Y, Wang LH (2007) Fluorescence sensing and binding behavior of amino benzene sulfonamidoquinolino ß-cyclodextrin to Zn^{2+}. Org Lett 9:315–318
7. Singh TS, Paul PC, Pramanik HAR (2014) Fluorescent chemosensor based on sensitive Schiff base for selective detection of Zn^{2+}. Spectrochim Acta A Mol Biomol Spectrosc 121:520–526
8. Xu Z, Yoon J, Spring DR (2010) Fluorescent chemosensors for Zn^{2+}. Chem Soc Rev 39:1996–2006
9. Jin Y, Wang S, Zhang Y, Song B (2016) Highly selective fluorescent chemosensor based on benzothiazole for detection of Zn^{2+}. Sensors Actuators B Chem 225:167–173
10. Gharami S, Aich K, Patra L, Mondal TK (2018) Detection and discrimination of Zn^{2+} and Hg^{2+} using a single molecular fluorescent probe. New J Chem 42:8646–8652
11. Choi JY, Kim D, Yoon J (2013) A highly selective "turn-on" fluorescent chemosensor based on hydroxy pyrene–hydrazone derivative for Zn^{2+}. Dyes Pigments 96:176–179
12. Zhou X, Lu Y, Zhu JF, Chan WH, Lee AW, Chan PS, Wong RN, Mak N (2011) Ratiometric fluorescent Zn^{2+} chemosensor constructed by appending a pair of carboxamidoquinoline on 1,2-diaminocyclohexane scaffold. Tetrahedron 67:3412–3419
13. Zhou X, Yu B, Guo Y, Tang X, Zhang H, Liu W (2010) Both visual and fluorescent sensor for Zn^{2+} based on quinoline platform. Inorg Chem 49:4002–4007
14. Xu Z, Liu X, Pan J, Spring DR (2012) Coumarin-derived transformable fluorescent sensor for Zn^{2+}. Chem Commun 48:4764–4766
15. Fu ZH, Yan LB, Zhang X, Zhu FF, Han XL, Fang J, Wang YW, Peng Y (2017) A fluorescein-based chemosensor for relay fluorescence recognition of cu(II) ions and biothiols in water and its applications to a molecular logic gate and living cell imaging. Org Biomol Chem 15:4115–4121
16. Anand T, Ashok Kumar SK, Sahoo SK (2018) A new Al^{3+} selective fluorescent turn-on sensor based on hydrazide-naphthalic anhydride conjugate and its application in live cells imaging. Spectrochim Acta A 204:105–112
17. Basabe-Desmonts L, Reinhoudt DN, Crego-Calama M (2007) Design of fluorescent materials for chemical sensing. Chem Soc Rev 36:993–1017
18. Erdemir S, Malkondu S (2016) Design of Luminescent Materials with "turn-on/off" response for anions and cations. Adv Magnetic Opt Mater:279–308
19. Sasaki H, Hanaoka K, Urano Y, Teraia T, Nagano T (2011) Design and synthesis of a novel fluorescence probe for Zn^{2+} based on the spirolactam ring-opening process of rhodamine derivatives. Bioorg Med Chem 19:1072–1078
20. Gao Y, Liu H, Li P, Liu Q, Wang W, Zhao B (2017) Coumarin-based fluorescent chemosensor for the selective quantification of Zn^{2+} and AcO^{-} in an aqueous solution and living cells. Tetrahedron Lett 58:2193–2198
21. Roy I, Shin JY, Shetty D, Khedkar JK, Park JH, Kim K (2016) E-Bodipy fluorescent chemosensor for Zn^{2+} ion. J Photochem Photobiol A Chem 331:233–239
22. Erdemir S, Tabakci B (2017) Selective and sensitive fluorescein-Benzothiazole based fluorescent sensor for Zn^{2+} ion in aqueous media. J Fluoresc 27:2145–2152
23. Andra SS, Charisiadis P, Arora M, Vliet-Ostaptchouk JV, Makris KC (2015) Biomonitoring of human exposures to chlorinated derivatives and structural analogs of bisphenol a. Environ Int 85:352–379
24. Erdemir S, Yuksekogul M, Karakurt S, Kocyigit O (2017) Dual-channel fluorescent probe based on bisphenol A-rhodamine for Zn^{2+} and Hg^{2+} through different signaling mechanisms and its bioimaging studies. Sensors Actuators B Chem 241:230–238
25. Erdemir S, Kocyigit O, Malkondu S (2015) Fluorogenic recognition of Zn^{2+}, Al^{3+} and F^{-} ions by a new multi-Analyte Chemosensor based bisphenol A-Quinoline. J Fluoresc 25:719–727
26. Wu J, Sheng R, Liu W, Wang P, Zhang H, Ma J (2012) Fluorescent sensors based on controllable conformational change for discrimination of Zn^{2+} over Cd^{2+}. Tetrahedron 68:5458–5463
27. Feng ET, Tu YY, Fan CB, Liu G, Pu SZ (2017) A highly selective and sensitive fluorescent chemosensor for Zn^{2+} based on a diarylethene derivative. RSC Adv 7:50188–50194
28. Benesi HA, Hildebrand J (1949) A spectrophotometric investigation of the interaction of iodine with aromatic hydrocarbons. J Am Chem Soc 71(8):2703–2707
29. Frisch MJ, Trucks GW, Schlegel HB, Scuseria GE, Robb MA, Cheeseman JR, Scalmani G, Barone V, Petersson GA, Nakatsuji H, Li X, Caricato M, Marenich AV, Bloino J, Janesko BG, Gomperts R, Mennucci B, Hratchian HP, Ortiz JV, Izmaylov AF, Sonnenberg JL, Williams-Young D, Ding F, Lipparini F, Egidi F, Goings J, Peng B, Petrone A, Henderson T, Ranasinghe D, Zakrzewski VG, Gao J, Rega N, Zheng G, Liang W, Hada M, Ehara M, Toyota K, Fukuda R, Hasegawa J, Ishida M, Nakajima T, Honda Y, Kitao O, Nakai H, Vreven T, Throssell K, Montgomery JA, Jr., Peralta JE, Ogliaro F, Bearpark MJ, Heyd JJ, Brothers EN, Kudin KN, Staroverov VN, Keith TA, Kobayashi R, Normand J, Raghavachari K, Rendell AP, Burant JC, Iyengar SS, Tomasi J, Cossi M, Millam JM, Klene M, Adamo C, Cammi R, Ochterski JW, Martin RL, Morokuma K, Farkas O, Foresman JB, and Fox DJ, Gaussian, Inc., Wallingford CT, 2016
30. Becke AD (1993) Density- functional thermochemistry. III. The role of exact exchange. J Chem Phys 98:5648–5652
31. Lee C, Yang W, Parr RG (1988) Development of the Colle-Salvetti correlation-energy formula into a functional of the electron density. Phys rev [sect.] B. 37:785
32. Shuangchen M, Huihui S, Bin Z, Gongda C, Zhu S (2013) Experimental study of co(II) additive on ammonia escape in carbon capture using renewable ammonia. Chem Eng J 34:430–436